RSC Advances

ROYAL SOCIETY OF CHEMISTRY

www.rsc.org/advances

RSC Advances

RSCPublishing

ARTICLE

Synthesis and CO gas sensing properties of surface-nitridated Ga_2O_3 nanowires

Cite this: *RSC Adv.*,

S. H. Park, S. H. Kim, S. Y. Park and C. Lee

Ga_2O_3 based gas sensors have limited use at a temperature lower than 400°C because of their poor performances at low temperatures. Efforts to improve their performances at room temperature further are necessary. This study examined the sensing properties of surface-nitridated Ga_2O_3 nanowires toward CO gas. Surface-nitridated Ga_2O_3 nanowires were fabricated by thermal evaporation of GaN powders followed by thermal nitridation in an NH_3 atmosphere. Scanning electron microscopy and transmission electron microscopy showed that the GaN shell layer in a typical surface- nitridated nanowire had a thickness of ~21 nm and excellent shell layer thickness uniformity. Multiple networked surface-nitridated Ga_2O_3 nanowire sensors showed responses of 160-363% to CO concentrations of 10-200 ppm at 150°C. These responses were 1.6-3.1 fold stronger than those of pristine Ga_2O_3 nanowire sensors at the same CO concentrations and stronger than those of many pristine metal oxide nanostructures and Ga_2O_3/metal oxide core-shell nanowires at similar temperatures. The results showed that the sensitivity of Ga_2O_3 nanowire could be enhanced by simple amoniation treatment. The enhanced response of the surface-nitridated Ga_2O_3 nanowires to CO gas can be explained based on a potential barrier carrier transport mechanism combined with a surface depletion mechanism and the excellent shell layer uniformity.

DOI: 10.1039/x0xx00000x

www.rsc.org/

1. Introduction

Monoclinic gallium oxide (β-Ga_2O_3)-based gas sensors show high electrical conductivity and recombination activity at high temperatures of 600–1000°C [1,2]. They showed strong responses to reducing gases such as H_2, CO, CH_4, etc. at high temperatures. On the other hand, they showed poor conductivity at room temperatures because of diffusion of oxygen-vacancies being frozen[3,4], which limits their application in the gas sensor field. A couple of techniques such as controlled doping and generation of defects (e.g., oxygen vacancies, surface atom coordination, or localized strain regions) have been tried to overcome this limitation.[5] A small amount of SnO_2 incorporation into Ga_2O_3 is known to increase the electrical conductivity and improve the CO and CH_4 gas sensitivity.[6,7]

The gas sensing properties of Schottky diode sensors based on Ga_2O_3 have been reported previously. The hydrogen sensing properties were measured in the range of 300-500°C. Trinnch et al. (2004) proposed a sensor with Pt/Ga_2O_3/SiC structure for the first time and demonstrated hydrogen sensing properties due to a change in Schottky barrier height[8]. Recently, Nakagoni et al. reported that the forward current was significantly increased upon exposure to hydrogen without showing the sensitivity[9], but there is no report on CO gas detection using Ga_2O_3-based Schottky diode sensors. The drawbacks of Schottky diode sensors are the relatively low reverse voltage ratings for silicon-metal Schottky diodes, and thermal instability due to a relatively high reverse leakage current[10]. In contrast, multiple-networked 1D nanostructured gas sensors have merits of simpler fabrication processes, superior reproducibility, and low fabrication cost.

In recent years, one-dimensional (1D) nanostructure-based sensors have been studied extensively because they show higher sensitivity, rapid response and superior spatial resolution due to their high surface-to-volume ratios compared to thin film gas sensors[11-13]. Considerable efforts have been made to develop 1D nanostructured gas sensors with good sensing performance, but further improvements in the sensitivity of 1D nanostructured sensors are needed for achieving satisfactory sensitivity. Several techniques such as doping[14-16], surface functionalization[17-19] and core-shell structure formation[20-22] are employed commonly to enhance the sensing performances of 1D nanostructure sensors. Among these techniques, the core-shell structure formation

technique was adopted to overcome the poor performance of the Ga_2O_3 1D nanostructure-based sensors at room temperature in this study. Jang et al. synthesized Ga_2O_3-core/SnO_2–shell nanowires by combining thermal evaporation and atomic layer deposition (ALD) and examined their ethanol-sensing properties. The networked core-shell nanowire sensors showed an order of magnitude higher gas response toward ethanol against other gases, such as H_2, CO, and NH_3. Liu et al. examined the CO gas sensing properties of multiple-networked Ga_2O_3 nanowire sensors in a temperature range of 100-500 °C and reported that the optimum operation temperature for CO sensing is 200 °C[23]. Kim et al. reported that the response of multiple-networked Ga_2O_3 nanowire sensors was enhanced ~17 fold by functionalizing them with Pt nanoparticles[24]. This study synthesized Ga_2O_3-core/GaN-nanowires by directly nitridating the surface of Ga_2O_3 nanowires and examined their sensing properties towards CO gas at 150°C. The results showed that the sensitivity of Ga_2O_3 nanowire could be considerably improved by a simple amoniation treatment.

2. Experimental

Surface-nitridated Ga_2O_3 nanowires were synthesized by thermal evaporation of GaN powders in an oxidizing atmosphere followed by thermal nitridation of Ga_2O_3 nanowire surface in an NH_3 atmosphere. Au-coated sapphire (Al_2O_3) was used as a substrate for the synthesis of 1D Ga_2O_3 structures. A 3 nm thick Au thin film was coated on the (100) Si substrate by a radio frequency (RF) magnetron sputtering technique. A quartz tube was mounted horizontally inside a tube furnace. The Au-coated Sapphire (Al_2O_3) substrate was placed downstream in the quartz tube, ~5 mm away from the GaN powders. After evacuating the quartz tube, the furnace was heated to 1,000°C and kept at that temperature for 1 h in N_2 /3mol%-O_2 atmosphere with constant flow rates of oxygen (O_2) (15 sccm) and N_2 (485 sccm). The total pressure was 1.5 Torr. The as-synthesized Ga_2O_3 nanowires were transferred to an annealing chamber. Nitridation was conducted on the surfaces of nanowires by heating at 900°C for 5 min in an NH_3 atmosphere. The NH_3 gas flow rate and pressure in the chamber were set to 50 cm^3/min and 0.5 Torr, respectively.

The morphology and structure of the products were characterized by scanning electron microscopy (SEM, Hitachi S-4200) operating at 10 kV and transmission electron microscopy (TEM, JEOL 2100F) with an accelerating voltage of 200 kV equipped with energy-dispersive X-ray spectroscopy (EDXS, EDAX) and selected area electron diffraction. The TEM samples were prepared by placing a small droplet (~10 μl) of diluted reaction solutions for 20 times on copper grids coated with amorphous carbon, and then heating the solvent at 40°C for 24 h. The TEM diffraction patterns were recorded through microdiffraction on individual nanowires. X-ray diffraction (Philips X'pert MRD) was performed using Cu Kα radiation (0.15406 nm) at a scan rate of 4°/min. The sample was arranged geometrically at a 0.5° glancing angle with a rotating detector. EDXS was carried out to confirm the structure of the nitridated Ga_2O_3 nanowire samples.

Nanowire samples were dispersed ultrasonically in a mixture of deionized water (5 mL) and isopropyl alcohol (5 mL), and dried at 90 °C for 30 min. A slurry droplet containing the nanowires (10 μL) was placed onto the SiO_2-coated Si substrates equipped with a pair of interdigitated (IDE) Ni(≈200 nm)/Au (≈50 nm) electrodes with a gap of 20 μm. A flow-through technique was used to test the gas sensing properties of the multiple networked pristine Ga_2O_3 nanowire and nitridated Ga_2O_3 nanowire sensors. CO gas diluted with synthetic air at different ratios was injected into the testing tube at a constant flow rate of 200 cm^3/min. The resistance in the sensors was measured using a Keithley sourcemeter-2612 under the source voltage of 10 V at 150°C under 50% RH. Detailed procedures for sensor fabrication and the sensing test are reported elsewhere[20].

3. Results and discussion

Fig. 1(a) shows SEM images of the surface-nitridated Ga_2O_3 1D nanostructures with a fiber-like morphology synthesized in this study. The nanowires were 50-150 nm in diameter and up to one millimeter in length. Fig. 1(b) presents the XRD patterns of the as-synthesized surface-nitridated Ga_2O_3 nanowires. The main reflection peaks in the pattern of the surface-nitridated Ga_2O_3 nanowires were assigned to a monoclinic structure, which is in good agreement with the data reported for bulk β-Ga_2O_3 crystals (JCPDS card No. 43-1012, a = 1.223 nm, b = 0.304 nm, c = 0.580 nm, β = 103.7°). In addition, two small reflection peaks for (111) and (220) GaN were also identified, suggesting that the nitride nanowires have crystalline Ga_2O_3 cores and crystalline GaN shells.

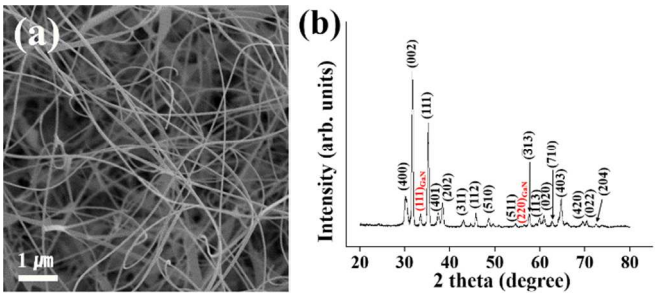

Fig. 1. (a) SEM image and (b) XRD pattern of surface-nitridated Ga_2O_3 nanowires.

Fig. 2(a) shows a low-magnification TEM image of a typical surface-nitridated Ga_2O_3 nanowire. The difference in contrast between the Ga_2O_3 core region and the GaN cell regions reveals that the core diameter and the shell layer thickness in the core-shell nanowire were approximately 75 nm and 21 nm, respectively. The shell layer showed a perfectly straight interface and excellent thickness uniformity along the nanowire length direction. Generally, the metal oxide / metal oxide core-shell heterostructure nanowires synthesized using a two-step process do not show such excellent shell layer thickness uniformity. Fig. 2(b) shows a local high-resolution TEM (HRTEM) image of the core-shell interfacial region of the nanowire. A closer examination revealed fringes both in the core (darker region on the lower left side) and the shell (lighter region on the upper right side). Two types of fringes parallel to Ga_2O_3 (111) and (002) lattice planes and one type of fringe parallel to GaN (111) lattice plane were observed in the core and shell regions, respectively. The corresponding selected area of electron diffraction (SAED) pattern (Fig. 2(c)) was recorded perpendicular to the long axis and indexed to the $[1\bar{1}1]$ zone axis of β-Ga_2O_3. The strong reflection spots in the SAED pattern were identified as the (002) and (111) reflections of monoclinic-structured Ga_2O_3, confirming that the Ga_2O_3 core was a single crystal. On the other hand, the dim reflection spots were assigned to the reflections from GaN. The dim reflection spots for GaN observable in the SAED pattern suggested that the GaN shell layer was also a single crystal, but no concentric ring pattern was observed. The line-scanning EDXS concentration profile across the diameter of a typical Ga_2O_3-core/GaN-shell nanowire (Fig. 2(d)) confirmed the core-shell structure by showing a higher oxygen concentration in the central

region and higher nitrogen concentrations in the edge regions. Despite this, a high nitrogen concentration was observed in the central region. The GaN shells on the front and rear sides as well as the Ga_2O_3 core in the central region were overlapped in the X-ray beam direction because a nanowire has a circular cylinder structure[25] as shown in Fig. 2(e). Therefore, both oxygen and nitrogen was detected in the central region. X-ray photoemission spectroscopy (XPS) was performed to confirm formation of a GaN layer on the surface of the Ga_2O_3 nanowires and the XP spectrum is shown in Fig. 2(f). The N1s peak at ~378 eV and the O1s peak at ~530.8 eV indicate formation of GaN and Ga_2O_3 phases, respectively. The Ga2p peak at ~1117.8 eV also indicates a Ga_2O_3 phase.

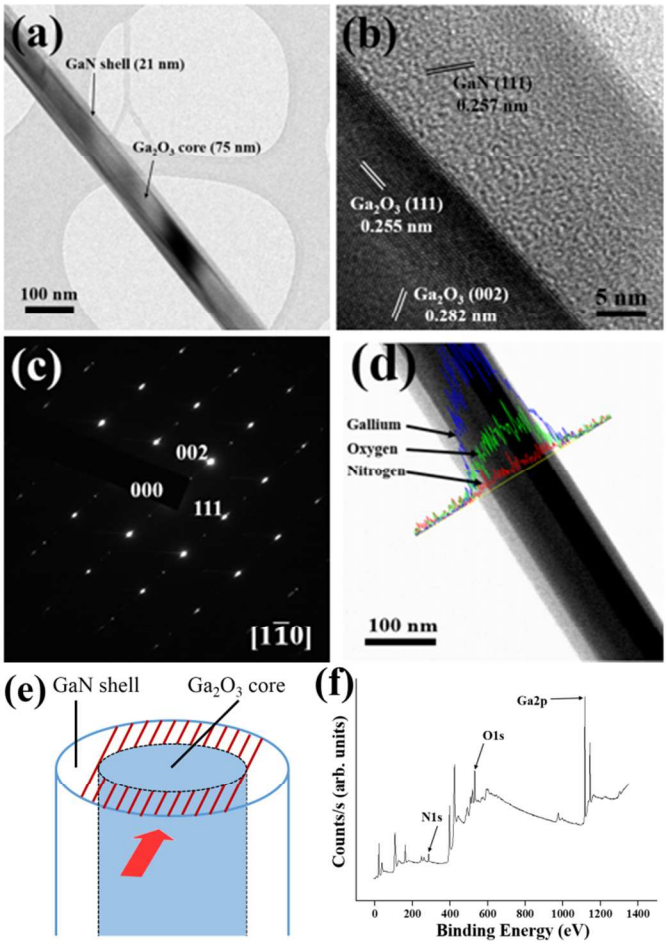

Fig. 2. (a) Low-magnification TEM image of typical nitridated Ga_2O_3 nanowire. (b) Local HRTEM image of the nanostructure at the core-shell interface region. (c) SAED pattern of the [1$\bar{1}$0] zone axis of the nanomaterials in the same region as in HRTEM. (d) Line-scanning EDXS concentration profile along the diameter of a typical nitride Ga_2O_3 nanowire. (e) Schematic showingthe overlap of GaN/Ga2O3/GaN layer in the central region of the EDXS. (f) XP spectrum of a typical surface-nitridated Ga_2O_3 nanowire.

Figs. 3(a) and 3(b) show the transient electrical responses of pristine Ga_2O_3 nanowires and surface-nitridated Ga_2O_3 nanowires, respectively, at an operating temperature of 150°C to a typical reducing gas CO. The sensors were exposed to successive pulses of 10 to 200 ppm CO gas. For different CO concentrations the resistance reached its original value after the CO gas flow was switched off, confirming that the absorption and desorption processes are reversible. Upon introduction of CO square pulses, the experimental curves in Figs. 3(a)-(b) increase sharply and subsequently more slowly up to the end of the pulse. This difference between the response time and recovery time might be due to the difference in solubility between CO and O_2.The solubility of CO in Ga_2O_3 or GaN might be larger than that of O_2 in Ga_2O_3 or GaN. Therefore, CO molecules are more easily adsorbed by the Ga_2O_3 or GaN surface upon exposure to CO gas than O_2 molecules upon exposure to air, resulting in a difference between response and recovery times.

The relative responses of the n-type pristine and surface-nitridated Ga_2O_3 nanowire sensors were defined as $[(R_g-R_g)/R_g]\times100\%$ for Ga_2O_3, where R_a and R_g are the electrical resistances of the sensors in air and CO gas, respectively. Fig. 3(c) shows the electrical responses of the pristine Ga_2O_3 and nitridated Ga_2O_3 nanowire sensors as a function of CO concentration. The pristine Ga_2O_3 nanowires showed responses of approximately 103-119% at CO concentrations of 10-200 ppm. In contrast, surface-nitridated Ga_2O_3 nanowires showed responses of 160-363% over the same concentration range. Therefore, the responses of the nitride Ga_2O_3 nanowires to 10-200 ppm CO were 1.6-3.1 times stronger than the pristine Ga_2O_3 nanowires. The increasing response rate as well as the higher response of the surface-nitridated Ga_2O_3 nanowire sensor according to the CO concentration compared to those of the pristine Ga_2O_3 nanowire sensor, respectively, suggests that the former would show a stronger response than the latter at the CO concentrations higher than 200 ppm as well as in the range of 10-200 ppm. The response of the surface-nitridated Ga_2O_3 nanowire sensor to 100 ppm of CO gas measured in this study was ~301%, which is far higher than ~112% obtained using the Pt-functionalized Ga_2O_3 nanowire sensor.[24]

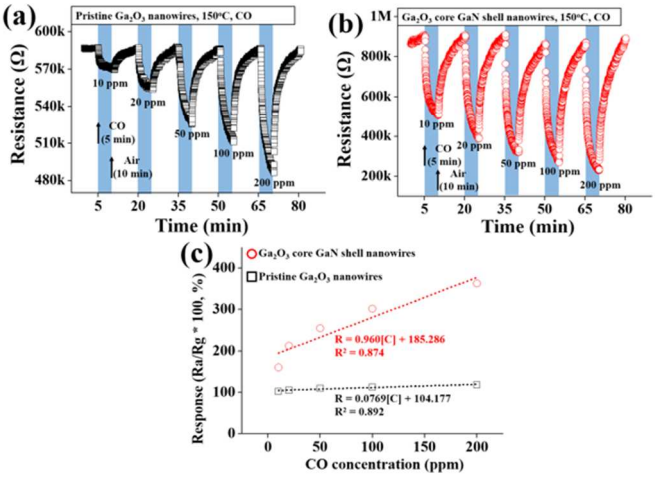

Fig. 3 Dynamic electrical responses of (a) pristine Ga_2O_3 nanowire sensor and (b) surface-nitridated Ga_2O_3 nanowire sensor. (c) Electrical responses of the pristine Ga_2O_3 nanowire sensor and the surface-nitridated Ga_2O_3 nanowire sensor as a function of CO concentration.

The technique of formation of core–shell nanostructures is more efficient for the detection of reducing gases such as CO, H_2, ethanol, etc. than for the detection of oxidizing gases such as NO_2 and O_2 [26,27]. The substantial improvement in the response of the Ga_2O_3 nanowires to CO gas by the nitridation of their surfaces can be explained by a combination of a potential barrier carrier transport mechanism[28,29] and a surface-depletion model[30,31] as well as the excellent GaN shell layer uniformity. First, according to the space-

charge model the sensing mechanism in the surface-nitridated Ga_2O_3 nanowire can be explained as follows:
In air, oxygen molecules are chemsorbed on the GaN shell surface of the nitridated nanowire and form oxygen ions by extracting electrons from the conduction band of GaN. These reactions produce an electron depletion layer near the GaN shell surface, leading to an increase in resistance. The width of the surface depletion layer is the order of Debye length λ_D, when the nitridated nanowire is exposed to air. Upon exposure to CO gas, the CO gas is adsorbed on the core-shell nanowire sensor and the electrons released from the adsorbed CO molecules are attracted to the GaN shell layer because a reducing gas such as CO acts as an electron donor in the reaction. This reaction will result in a decrease in the depletion layer width and a decrease in the resistance of the nanowire sensor. In other words, the depletion region shrinks significantly upon exposure to CO gas. In air, the depletion layer width in the surface-nitridated Ga_2O_3 nanowire is larger than that in the pristine nanowire. The Ga_2O_3-GaN interface in the nitridated nanowire contains a high density of interface states. The carriers near the interface are trapped by the interface, so a depletion layer forms in both the Ga_2O_3 core and GaN shell regions near the interface. Two different depletion layers form: one with a width equal to $\lambda_1 + \lambda_2$ in the interfacial region and the other with a width equal to λ_2 in the surface region in the nitridated nanowire, where λ_1 and λ_2 are the Debye lengths of Ga_2O_3 and GaN, respectively, as shown in Fig. 4. We prepared a thin film on a Si (100) substrate and calculated λ_1 in a similar manner in reference 19 and found λ_1= ~14.8 nm. The calculated Debye length of Ga_2O_3, λ_1 = ~14.8 nm and the Debye length of GaN, λ_2 found in the literature was ~10 nm[32].

In contrast, only a depletion layer with a width of λ_{D1} is created in a pristine Ga_2O_3 nanowire in air. Therefore, the total depletion layer width in a surface-nitridated Ga_2O_3 nanowire in air will be far larger than that in a pristine Ga_2O_3 nanowire, which would result in a greater change in the resistance of the surface-nitridated Ga_2O_3 nanowire than that of the pristine Ga_2O_3 nanowire.

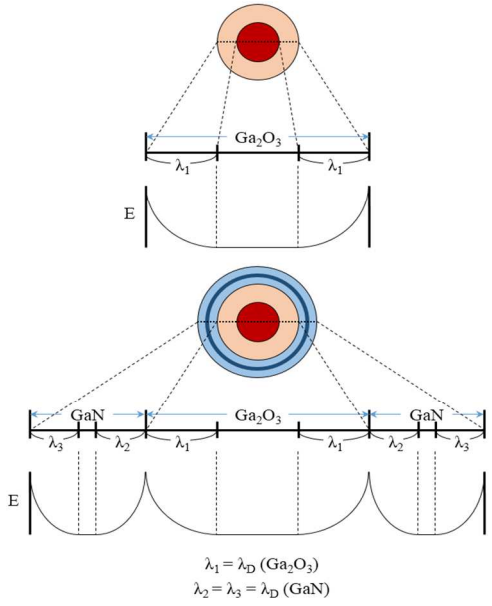

Fig. 4. Depletion layers and potential barriers created in surface-nitridated Ga_2O_3 nanowires. λ_1 = ~14.8 nm and λ_2 = ~10 nm[32], where λ_1 and λ_2 (= λ_3) are the Debye lengths of Ga_2O_3 and GaN, respectively.

A comparison of Figs. 3(a) and (b) reveals that the surface-nitridated Ga_2O_3 nanowires showed a larger change in resistance between exposure to air and exposure to CO gas, i.e., a stronger response or a higher sensitivity to CO compared with the pristine Ga_2O_3 nanowires. Upon exposure to air the resistance of, the surface-nitridated Ga_2O_3 nanowires is higher than that of the pristine Ga_2O_3 nanowires. On the other hand, upon exposure to the resiatance of the former is lower than the latter. This difference can also be explained based on the surface-depletion model. Upon exposure to air, The depletion layer width is much larger in the surface-nitridated Ga_2O_3 nanowires than in the pristine Ga_2O_3 nanowires. Therefore, the resistance of the former is higher than the latter. On the other hand, upon exposure to CO gas, the resistance of the surface-nitridated Ga_2O_3 nanowires is lower than that of the pristine Ga_2O_3 nanowires because the depletion layer reduction is more significant in the former than in the latter.

On the other hand, according to the potential barrier carrier transport mechanism the sensing mechanism of the surface-nitridated nanowires can be explained as follows:
A potential barrier is created at the core-shell interface due to carrier trapping, as shown in Fig. 4. Modulation of the potential barrier height at the Ga_2O_3-GaN interface occurs upon adsorption and desorption of gas molecules. Carrier transport is facilitated or restrained because of this potential barrier, resulting in a larger change in resistance, i.e., an enhanced response of the core-shell nanowire sensor to CO gas. Another type of potential barrier exists at the contact of two nanowires in a multiple networked surface-nitridated Ga_2O_3 nanowire sensor in addition to that built at the Ga_2O_3-core/GaN-shell interface (Fig. 4). The enhanced sensing performance of the sensor can be attributed to both types of potential barriers. The contribution of the potential barrier at the core-shell interface must be far greater than that of the potential barrier at the contact of two nanowires because the number of core-shell interfaces is far larger than that of the other. Overall, the enhanced responses of the surface-nitridated Ga_2O_3 nanowire sensor to CO gas can be attributed to modulations of the depletion layers and potential barriers induced by the adsorption and desorption of CO molecules.

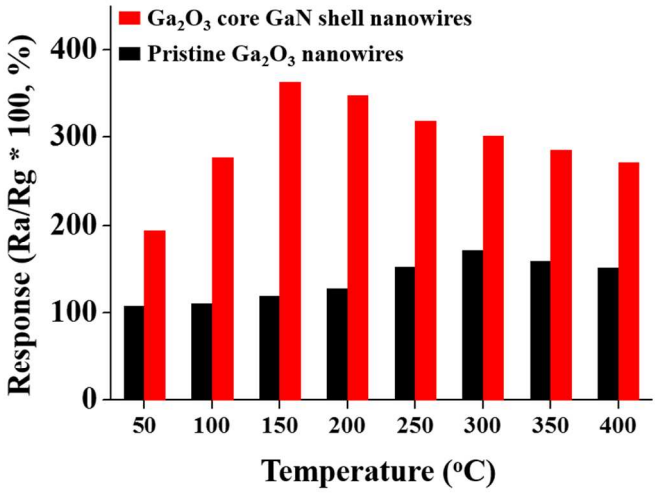

Fig. 5. Responses of the pristine Ga_2O_3 nanowire sensor and the surface-nitridated Ga_2O_3 nanowire sensor to 200 ppm of CO gas at different operating temperatures.

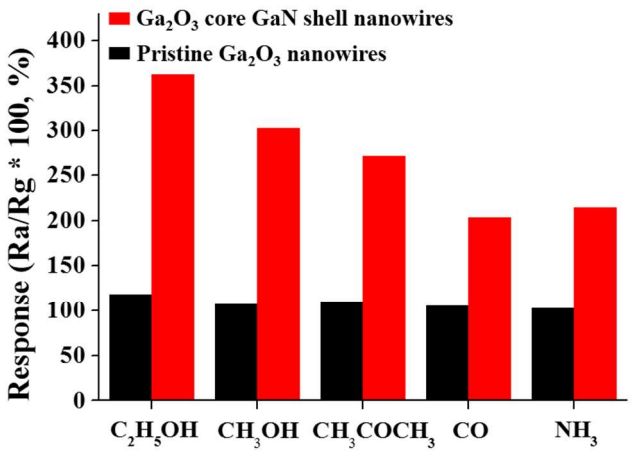

Fig. 6. Responses of the pristine Ga_2O_3 nanowire sensor and the surface-nitridated Ga_2O_3 nanowire sensor to 200 ppm of different gases at 150°C.

Fig. 5 shows the response of the response of the pristine and surface-nitrided Ga_2O_3 nanowire sensors to 200 ppm ethanol for different operating temperatures. A maximum response was obtained at 300 and 150, for the pristine and surface-nitrided Ga_2O_3 nanowire sensors, respectively. This result suggests that ammoniation treatment decreases the optimum operating temperature of the Ga_2O_3 nanowire sensor as well as enhances the sensitivity towards ethanol gas. Fig. 6 compares the response of the pristine and surface-nitrided Ga_2O_3 nanowire sensors to a range of gases. The pristine Ga_2O_3 nanowire sensor shows similar responses to five different gases. In contrast, the surface-nitrided Ga_2O_3 nanowire sensor shows the strongest response to ethanol than to the other gases, i.e., a high selectivity towards ethanol. This result suggests that the selectivity might be mainly attributed to the affinity of the GaN layer to ethanol.

4. Conclusions

Surface-nitridated Ga_2O_3 nanowires were fabricated by thermal evaporation of GaN powders followed by thermal nitridation in an NH_3 atmosphere. The ammoniation treatment resulted in a very uniform single crystal GaN layer with a thickness of ~ 21 nm on the surface of the nanowires. The ammoniation treatment improved the CO gas sensing properties of Ga_2O_3 nanowire remarkably. The enhanced response of the surface-nitridated Ga_2O_3 nanowires to CO gas can be attributed to the modulation of the potential barriers built at two different places in the multiple networked the surface-nitridated Ga_2O_3 nanowire sensors: the Ga_2O_3-GaN heterojunction at the core-shell interface and the contact point of two different core-shell nanorods. The results show that the sensitivity of multiple-networked Ga_2O_3 nanowire sensors could be enhanced significantly by simple amoniation treatment.

Acknowledgements

This research was supported by Basic Science Research Program through the National Research Foundation of Korea (NRF) funded by the Ministry of Education (2010-0020163).

Notes and references

Department of Materials Science and Engineering, Inha University, 253 Yonghyun-dong, Nam-gu, Incheon 402-751, Republic of Korea. Tel: +82 32 860 7536; E-mail: cmlee@inha.ac.kr

1 A. Kolmakov, Y. Zhang, G. Cheng and M. Moskovits, *Adv. Mater.,* 2003, **15**, 997.
2 Y. Liu, E. Koep and M. Liu, *Chem. Mater.,* 2005, **17**, 3997.
3 M. Law, H. Kind, B. Messer, F. Kim and P. Yang, *Angew. Chem.,* 2002, **41**, 2405.
4 Y. Lin, M. Huang, C. Liu, J. Chen, J. Wu and H. Shih, *J. Electrochem. Soc.,* 2009, **156**, K196.
5 N. Ramgir, I. Mulla and K. Vijayamohanan, *Sens. Actuators B: Chem*., 2005, **107**, 708.
6 T. Schwebel, M. Fleischer and H. Meixner, *Sens. Actuators B: Chem*., 2000, **65,** 176.
7 M. Ogita, K. Higo, Y. Nakanishi and Y. Hatanaka, *Appl. Surf. Sci.,* 2001, **175-176,** 721.
8 A. Trinch, W. Wlodarski and Y. Li, *Sens. Actuators B: Chem*., 2004, **100**, 94.
9 S. Nakagomi, K. Yokoyama and Y. Kobubun, *J. Sens. Sens. Syste.,* 2014, **3**, 231.
10 A. Kolmakov and M. Moskovits, *Ann. Rev. Mater. Res*., 2004, **34**, 151.
11 S. Park, S. An, H. Ko, C. Jin and C. Lee, *ACS Appl. Mater. Interfaces,* 2012, **4**, 3650.
12 M. Huang, S. Mao, H. Feick, H. Yan, Y. Wu, H. Kind, E. Weber, R. Russo and P. Yang, *Science*, 2001, **292**, 1897.
13 Y. Lin, M. Huang, C. Liu, J. Chen, J. Wu and H. Shih, *J. Electrochem. Soc.*, 2009, **156**, K196.
14 H. Kim, C. Jin, S. Park, S. Kim and C. Lee, *Sens. Actuators B: Chem*., 2012, **161**, 594.
15 N. Ramgir, I. Mulla and K. Vijayamohanan, *Sens. Actuators B: Chem*., 2005, **107**, 708.
16 Q. Wan and T. Wang, *Chem. Commun.*, 2005, **1**, 3841.
17 A. Kolmakov, D. Klenov, Y. Lilach, S. Stemmer and M. Moskovits, *Nano Lett*, 2005, **5**, 667.
18 Q. Kuang, C. Lao, Z. Li, Y. Liu, Z. Xie, L. Zheng and Z. Wang, *J. Phys. Chem. C*, 2008, **112**, 11539.
19 C. Jin, S. Park, H. Kim and C. Lee, *Sens. Actuators B: Chem*., 2012, **161**, 223.
20 S. Park, H. Ko, S. Kim and C. Lee, *ACS Appl. Mater. Interfaces,* 2014, **6**, 9595.
21 S. Park, S. An, Y. Mun and C. Lee, *ACS Appl. Mater. Interfaces*, 2013, **5**, 4285.
22 Z, Liu, T. Yamazaki, Y. Shen, T. Kikuta, N. Nakatani and Y. Li, *Sens. Actuators B: Chem*., 2008, **129**, 666.
23 H. Kim, C. Jin, S. An and C. Lee, *Ceram. Inter.*, 2012, **38**, 3563.
24 C. Jin, J. Lee, K. Baek and C. Lee, *Cryst. Res. Techno*., 2010, **45**, 1069.

25 N. Singh, A. Ponzoni, R. Gupta, P. Lee and E. Comini, *Sens. Actuators B: Chem.*, 2011, **160,** 1346.
26 A. Katoch, S. Choi, G. Sun and S. Kim, *J. Mater. Chem. A*, 2013, **1,** 13588.
27 L. Wang, Y. Kang, Y. Wang, B. Zhu, S. Zhang and W. Huang, *Mater. Sci. Eng. C*, 2012, **32,** 2079.
28 Y. Liu, G. Zhu, J. Chen, H. Xu, X. Shen and A. Yuan, *Appl. Surf. Sci.*, 2012, **265,** 379.
29 W. Wang, Z. Li, W. Zheng, H. Huang, C. Wang and J. Sun, *Sensors Actuators B: Chem.*, 2010, **143,** 754.
30 P. Sun, Y. Sun, J. Ma, L. You, G. Lu, W. Fu, M. Li and H. Yang, *Sens. Actuators B: Chem.*, 2011, **155,** 606.
31 H. Altunas, I. Donmez, C. Ozgit-Akgun and N. Biyikli, *J. All. Comp.*, 2014, **593,** 190.
32 A. Rizzi, M. Kocan, J. Malindretos, A. Schildknecht, K. Thonke and R. Sauer, *Appl. Phys. A*, 2007, **87,** 505.